Classical geometrical approach to circle fitting – review and new developments.

Article *in* Journal of Electronic Imaging · January 2003

DOI: 10.1117/1.1525792 · Source: DBLP

4 authors:

Corneliu Rusu
Universitatea Tehnica Cluj-Napoca
134 PUBLICATIONS **702** CITATIONS
SEE PROFILE

Marius Tico
Apple Inc.
63 PUBLICATIONS **1,725** CITATIONS
SEE PROFILE

Pauli Kuosmanen
Tampere University
125 PUBLICATIONS **2,391** CITATIONS
SEE PROFILE

Edward J. Delp
Purdue University
633 PUBLICATIONS **15,296** CITATIONS
SEE PROFILE

Journal of Electronic Imaging 12(1), 179–193 (January 2003).

Classical geometrical approach to circle fitting—review and new developments

Corneliu Rusu
Tampere University of Technology
Tampere International Center for Signal Processing
P.O. Box 553, FIN-33101
Tampere, Finland
and
Technical University of Cluj-Napoca
Department of Electronics and Telecommunications
Str. Baritiu Nr. 26-28, RO-3400
Cluj-Napoca, Romania

Marius Tico
Nokia Research Center
P.O. Box 100, FIN-33721
Tampere, Finland

Pauli Kuosmanen
Tampere University of Technology
Institute of Signal Processing
P.O. Box 553, FIN-33101
Tampere, Finland

Edward J. Delp
Purdue University
School of Electrical and Computer Engineering
West Lafayette, Indiana 47907-1285, USA

Abstract. *After a review of the circle fitting issue, we recall a relatively unknown method derived from a classical geometric result. We propose an improvement of this technique by reweighting the data, iterating the procedure, and choosing at every step as the new inversion point the one diametrically opposite to the previous inversion point.* © *2003 SPIE and IS&T.* [DOI: 10.1117/1.1525792]

1 Introduction

Fitting a circle to a set of noisy data points is an old problem that has motivated a large amount of—often duplicated—literature in various fields.[1] In many situations, what is perceived is not the complete locus of a circle, but a sample of points, where the noise is scattered about an arc of a circle.[2] It was suggested that the larger the angle, the better the precision of the estimated circle parameters, and also the variances become infinitely high when the arc angle approaches zero.[3] The presence of noise means also that an approximate way for fitting circles is required.[4] One of the oldest robust methods used in the recognition and extraction of circles from a digital image is the Hough transform. Unfortunately the Hough transform is suitable for problems having enough correct data to support the expected solution.[5] The orthogonal distance regression (ODR) method determines the curve that minimizes the sum of square of distances from each data point to the closest point on the curve. The ODR is well known to be computationally difficult. Another major drawback related to the general use of least squares is that they are sensitive to outliers.[6] If we enlarge the family addressed to the class of conics, then essentially two types of methods have been implemented for fitting.[7] The first one has been referred to as algebraic fitting, where the implicit form is used and the residual is minimized; the other is geometric fitting, where the goal is to minimize the sum of the squares of the distances between the scattered points and the conic. In the following, we shall understand by geometric approaches those techniques obtained by using some classical geometrical results. Thus their outcomes may finally belong from both either algebraic or geometric distance methods.

The goals of this paper are to briefly review a known method derived from a classical geometrical result and to

Paper JEI 01071 received Nov. 27, 2001; revised manuscript received Jun. 21, 2002; accepted for publication Aug. 13, 2002.
1017-9909/2003/$15.00 © 2003 SPIE and IS&T.

present a new technique based on this method. The proposed technique enables us to deal with and to fit a circle in a convenient form for scattered points when they are symmetrically and/or asymmetrically distributed around the circumference of the circle. The approach proposed is based on the property of an inversion transformation to map a circle into a straight line, if the circle passes through the pole of the inversion.[8] The idea was originally traced by Brandon and Cowley,[9] but it is relatively unknown. Our contribution consists of modifying the algorithm by weighting the data, iterating the procedure, and choosing at every step as the new inversion point the one diametrically opposite to the previous inversion point. The paper is organized as follows. Section 2 presents the previous geometrical approaches. Section 3 describes and analyses the inversion transformation method. Section 4 introduces the proposed weighting iterative method and provides the necessary information for implementing the procedure.

2 Previous Geometrical Approaches

In circle fitting, simple chord theorems for circles can be used,[9] as every circle is completely determined by three noncolinear points. From an algebraic point of view, the resulting matrix equation will be poorly conditioned if the matrix is singular or near singular, and this will happen if the data points are spread around a short arc. A least-squares error criterion for circle fitting results in minimizing the mean square error (MSE) sum

$$\mathrm{MSE}=\sum_{i=1}^{N}(R_i-R)^2, \tag{1}$$

where $R_i=[(x_i-A)^2+(y_i-B)^2]^{1/2}$. In this formula, (x_i,y_i) represent the (x, y) coordinates of the i'th data point, $N\geqslant 3$ is the number of data points, (A, B) are the coordinates of the circle center, and R is the radius of the circle.

It is quite easy to realize that the error criterion defined by Eq. (1) is difficult to handle analytically and one rather prefers to look for some other properties of the circle that in some way show how far is a certain point from the given circle. Indeed, if we consider minimizing the sum,

$$\sum_{i=1}^{N}(R_i^2-R^2)^2, \tag{2}$$

then we can easily get the formulas for the center and the radius of the circle (Fig. 1). This is the elegant geometric approach known as the Kasa method.[10] It has the following properties:

1. It is more advantageous to minimize not the mean squares [Eq. (1)], but R^2, whose contribution to Eq. (2) is more important.[11] This leads to a superfluous sensitivity to any small errors in measurements.
2. The Kasa procedure gives biased estimates of the circle center unless the data are symmetrically distributed around the circumference of the circle.
3. The bias is small and tends to 0 as the number of data points approaches infinity, i.e., the estimation is consistent. The accuracy obtained is related to the arc length and to the noise present in the data.
4. Arcs with larger radii fit more closely to the data than those with smaller radii.[2]

The case in which the data result in ambiguous circle and the circle fit must be rejected was considered in Ref. 12.

3 Inversion Method of Brandon and Cowley

In their method,[9] the authors recalled a well-known property of conformal mappings, precisely that circles through the origin map to straight lines under inversion. Thus if the data points $M_i(x_i,y_i)$ lie approximately on a circle, their images $N_i(u_i,v_i)$ will lie approximately on a straight line after inversion (Fig. 2). Therefore we can use a standard straight line fit formula (total least squares[13]) in the (u,v) coordinates. Taking the inverse of the fitted straight line using the same pole of inversion (also called inversion point or pivot point) $P(X,Y)$ we retrieve the fitted circle. Thus the algorithm that estimates a circle using this inversion transformation method[9] can be written as follows:

(I-1) Given
$N=$ number of points
$M_i(x_i,y_i)=$ data to be fitted by circle
$\rho=$ parameter of the inversion transformation I
$P(X,Y)=$ pole of inversion transformation I

(I-2) Compute the data $N_i(u_i,v_i)$ in the uv plane with:

$$u_i=X+\frac{(x_i-X)\rho^2}{(x_i-X)^2+(y_i-Y)^2},$$
$$v_i=Y+\frac{(y_i-Y)\rho^2}{(x_i-X)^2+(y_i-Y)^2}. \tag{3}$$

(I-3) Compute the parameters a and b of their fitted straight line $v=a+bu$ using total least squares method[13]:

$$a=\overline{v}-b\overline{u},$$
$$b=\frac{-(S_{uu}-S_{vv})+[(S_{uu}-S_{vv})^2+4S_{uv}^2]^{1/2}}{2S_{uv}}, \tag{4}$$

where

$$\overline{u}=\frac{1}{N}\sum_{i=1}^{N}u_i,\quad \overline{v}=\frac{1}{N}\sum_{i=1}^{N}v_i,$$
$$S_{uu}=\sum_{i=1}^{N}(u_i-\overline{u})^2,\quad S_{uv}=\sum_{i=1}^{N}(u_i-\overline{u})(v_i-\overline{v}), \tag{5}$$
$$S_{vv}=\sum_{i=1}^{N}(v_i-\overline{v})^2.$$

(1) Let denote by:

$$\Sigma_\alpha = 2[(\sum_{n=1}^{N} x_i)^2 - N\sum_{n=1}^{N} x_i^2];$$
$$\Sigma_\beta = 2[(\sum_{n=1}^{N} x_i)(\sum_{n=1}^{N} y_i) - N\sum_{n=1}^{N} x_i y_i];$$
$$\Sigma_\gamma = 2[(\sum_{n=1}^{N} y_i)^2 - N\sum_{n=1}^{N} y_i^2];$$
$$\Sigma_\delta = (\sum_{n=1}^{N} x_i^2)(\sum_{n=1}^{N} x_i) - N(\sum_{n=1}^{N} x_i^3) + (\sum_{n=1}^{N} x_i)(\sum_{n=1}^{N} y_i^2) - N(\sum_{n=1}^{N} x_i y_i^2);$$
$$\Sigma_\epsilon = (\sum_{n=1}^{N} x_i^2)(\sum_{n=1}^{N} y_i) - N(\sum_{n=1}^{N} y_i^3) + (\sum_{n=1}^{N} y_i)(\sum_{n=1}^{N} y_i^2) - N(\sum_{n=1}^{N} x_i^2 y_i).$$

(2) The coordinates of the center of the circle are:

$$A = \frac{\Sigma_\delta \Sigma_\gamma - \Sigma_\epsilon \Sigma_\beta}{\Sigma_\alpha \Sigma_\gamma - \Sigma_\beta^2}; \quad B = \frac{\Sigma_\alpha \Sigma_\epsilon - \Sigma_\beta \Sigma_\delta}{\Sigma_\alpha \Sigma_\gamma - \Sigma_\beta^2}.$$

(3) The radius of the circle is given by:

$$R^2 = A^2 + B^2 + \frac{1}{N}\left[\sum_{n=1}^{N} x_i^2 - 2A\sum_{n=1}^{N} x_i + \sum_{n=1}^{N} y_i^2 - 2B\sum_{n=1}^{N} y_i\right].$$

Fig. 1 Circle center (*A, B*) and radius *R* with the Kasa method.

(I-4) Find the fitted circle C^* that corresponds to the fitted straight line. For this aim we shall use I^{-1} the inverse of inversion transformation.[†] The steps are the following:

(a) For the given pole of inversion $P(X,Y)$ we have a certain point $P_{**}(X_{**},Y_{**})$ on a line $Y=a+bX$ that is closest when we measure distance orthogonally:

$$X_{**}=\frac{bY+X-ab}{1+b^2}, \quad Y_{**}=a+b\frac{bY+X-ab}{1+b^2}.$$

(b) The corresponding image point of $P_{**}(X_{**},Y_{**})$ by using I^{-1} is exactly $P^{**}(X^{**},Y^{**})$, the new diametrically opposite in the circle C^* to the $P(X,Y)$:

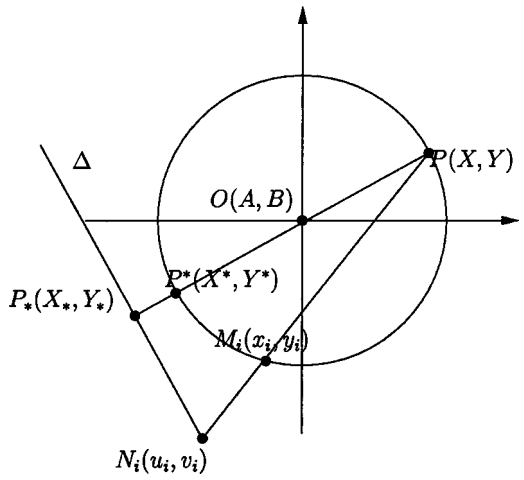

Fig. 2 Inversion of a circle when the pole lies on the circle.

[†]Actually $I^{-1}=I$ (Ref. 8).

Table 1 Data set for Example 1.

x	1	2	5	7	9	3
y	7	6	8	7	5	7

$$X^{**}=X+\frac{(X_{**}-X)\rho^2}{(X_{**}-X)^2+(Y_{**}-Y)^2},$$

$$Y^{**}=Y+\frac{(Y_{**}-Y)\rho^2}{(X_{**}-X)^2+(Y_{**}-Y)^2}.$$

(c) The fitted circle is described by the coordinates of the center $O^*(A^*,B^*)$ and the radius R^*:

$$A^*=\frac{X+X^{**}}{2},\quad B^*=\frac{Y+Y^{**}}{2},$$

$$R^*=[(X-A^*)^2+(Y-B^*)^2]^{1/2}.$$

3.1 *Examples*

3.1.1 *Example 1: The data set of Gander, Golub, and Strebel*[7]

Let us consider the pairs of points in Table 1. It is easy to show that they can not be located on same circle. These points were fitted in Ref. 7 by circles using different methods.

Minimizing the algebraic distance:

$A=5.3794,\quad B=7.2532,\quad R=3.0370,\quad \mathrm{MSE}=10.8532.$

Minimizing the geometric distance:

$A=4.7398,\quad B=2.9835,\quad R=4.7142,\quad \mathrm{MSE}=1.2276.$

This last one was considered there by the authors as the best circle fit (Fig. 3).

If someone would like to implement the Kasa method, the results are

$A=4.7423,\quad B=3.8351,\quad R=4.1088,\quad \mathrm{MSE}=1.3983.$

The differences can be explained by recalling that the Kasa method does not minimize in the mean square sense. In addition, the data are spread only on a third part of the best circle fit and as we have already pointed out, the Kasa method gives biased estimates of the circle center.[14]

Parameters of the fitted circles by inversion method for different inversion poles are also presented in Fig. 3:

$X=0,\ Y=1\ \ A=4.7020,\ B=2.6223,\ R=4.9740,$

$\mathrm{MSE}=1.2481,$

$X=9.5,\ Y=4:\ A=5.445,\ B=4.3129,\ R=4.0672,$

$\mathrm{MSE}=2.7624.$

The inversion constant has been selected $\rho=1$. We can conclude that the results depend on the choice of the inversion pole $P(X,Y)$ and with the inversion method, one can obtain better results than with the Kasa method, if the pole of inversion is proper selected. However, for a poor choice of inversion pole, the results can be depreciated.

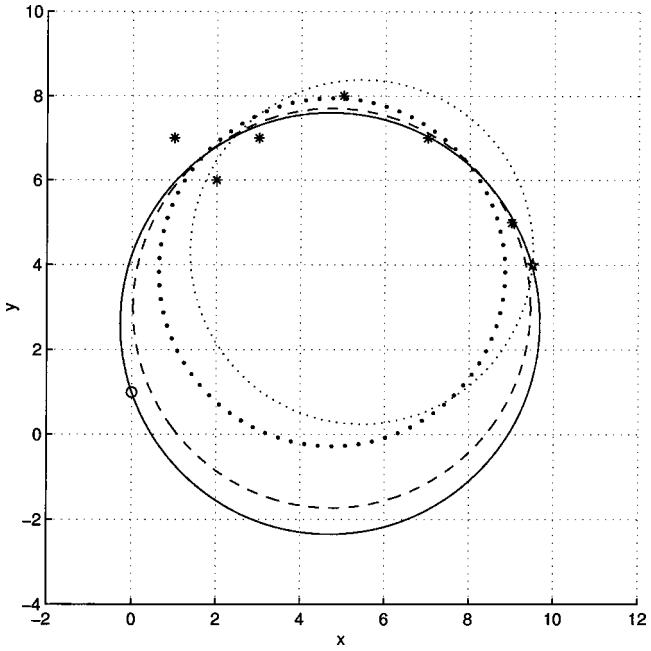

Fig. 3 Six points (*) from Example 1 with four fitted circles obtained using best fitted circle[7] (- -), Kasa method (·), and inversion method (–) when $P(0,1)$ (○) is inversion pole, and, respectively, (:) when $P(9.5,4)$ and (⋆) is inversion pole.

3.1.2 *Example 2: The pole of inversion and the localization of the scattered points*

The goal of this experiment is to show the manner in which the position of the pole of inversion and of the scattered points affects the circle-fitted parameters. For this reason, we select the same parameters of inversion, but we rotate the scattered points around the inversion circle, keeping the same geometric configuration for every trial. A random 10,000 trials are generated and the results averaged.

The parameters of inversion transformation are

1. The inversion circle has radius $R=1$ and its center is located at $O(0,0)$.
2. The pole of inversion is fixed at $P(-1,0)$.
3. The parameter of inversion is selected $\rho=1$.

The points are uniform distributed around the circle within an angle $\pi/8$. Their coordinates on x and y axes, respectively, of the distances to the circle are uniform distributed between ± 0.01. A random configuration is generated at the beginning and it is rotated around the circle 100 times, every time with an angle $2\pi/100$. For every case, we compute the new circle fitted with inversion transformation method. The MSE in circle radius and, respectively, in center position are later saved corresponding to the angle of rotation. Then another 9,999 trials are generated and the results averaged.

The outcome of such an experiment is presented in Fig. 4, where plots of the MSE for circle radius and circle center

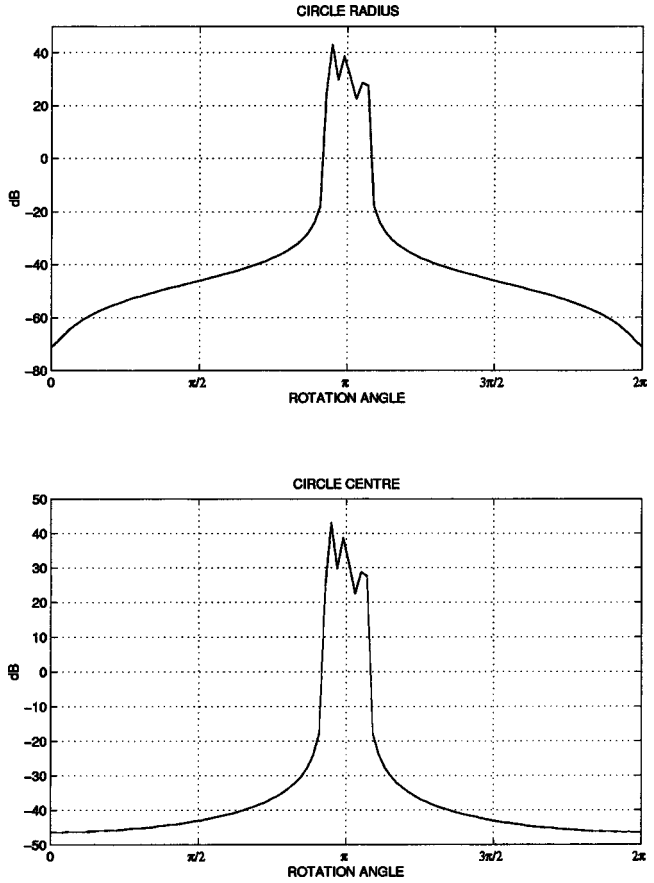

Fig. 4 MSE in decibels of the circle-fitted parameters (the radius and the center of the circles) for different scattered point rotation angles.

are provided. It is easy to see that for both of the mentioned parameters, the errors increase dramatically when the angle of rotation approaches π, i.e., when the scattered points are close to the pole of inversion. We can conclude that the inversion method as traced by Brandon and Cowley fails in such a situation. The following analysis gives more information about the behavior of the inversion transformation method and provides us with some tracks to follow to avoid some of its inconveniencies.

3.2 *Inversion Method Analysis*

Consider now the Cartesian model[15] of the given points $M_i(x_i, y_i)$:

$$x_i = A + R\cos\theta_i + \epsilon_i, \quad y_i = B + R\sin\theta_i + \delta_i, \tag{6}$$

where ϵ_i, δ_i, $i = 1,2,...,N$, are independent random errors with common variance, and θ_i are either fixed or random angles.

In a similar way we have for the pole of inversion:

$$X = A + R\cos\theta, \quad Y = B + R\sin\theta, \tag{7}$$

where θ is its corresponding angle. We can easily find now the coordinates of $P^*(X^*, Y^*)$ and $P_*(X_*, Y_*)$, the symmetric of the pole of inversion and its image under inversion:

$$\begin{aligned} X^* &= A + R\cos(\pi+\theta) = A - R\cos\theta, \\ Y^* &= A + R\sin(\pi+\theta) = B - R\sin\theta, \end{aligned} \tag{8}$$

$$\begin{aligned} X_* &= X + \frac{(X^*-X)\rho^2}{(X^*-X)^2+(Y^*-Y)^2} = A + R\cos\theta - \frac{\rho^2}{2R}\cos\theta, \\ Y_* &= Y + \frac{(Y^*-Y)\rho^2}{(X^*-X)^2+(Y^*-Y)^2} = B + R\sin\theta - \frac{\rho^2}{2R}\sin\theta. \end{aligned} \tag{9}$$

Now we focus on the computation of the last terms of Eqs. (3) using Eqs. (6) and (7). The outcomes are

$$\begin{aligned} \frac{(x_i-X)\rho^2}{(x_i-X)^2+(y_i-Y)^2} &= \frac{(R\cos\theta_i - R\cos\theta + \epsilon_i)\rho^2}{(R\cos\theta_i - R\cos\theta + \epsilon_i)^2 + (R\sin\theta_i - R\sin\theta + \delta_i)^2} \\ &= \frac{\rho^2}{2R}\,\frac{\cos\theta_i - \cos\theta + \epsilon_i/R}{1-\cos(\theta_i-\theta) + \epsilon_i/R(\cos\theta_i - \cos\theta) + \delta_i/R(\sin\theta_i - \sin\theta) + (\epsilon_i^2+\delta_i^2)/(2R^2)}, \end{aligned}$$

$$\begin{aligned} \frac{(y_i-Y)\rho^2}{(x_i-X)^2+(y_i-Y)^2} &= \frac{(R\sin\theta_i - R\sin\theta + \epsilon_i)\rho^2}{(R\cos\theta_i - R\cos\theta + \epsilon_i)^2 + (R\sin\theta_i - R\sin\theta + \delta_i)^2} \\ &= \frac{\rho^2}{2R}\,\frac{\sin\theta_i - \sin\theta + \delta_i/R}{1-\cos(\theta_i-\theta) + \epsilon_i/R(\cos\theta_i - \cos\theta) + \delta_i/R(\sin\theta_i - \sin\theta) + (\epsilon_i^2+\delta_i^2)/(2R^2)}. \end{aligned}$$

It follows from Eq. (3) that we have

$$\begin{aligned} u_i &= X + \frac{(x_i-X)\rho^2}{(x_i-X)^2+(y_i-Y)^2} \\ &= A + R\cos\theta + \frac{\rho^2}{2R}\,\frac{\cos\theta_i - \cos\theta + \epsilon_i/R}{1-\cos(\theta_i-\theta) + \epsilon_i/R(\cos\theta_i - \cos\theta) + \delta_i/R(\sin\theta_i - \sin\theta) + (\epsilon_i^2+\delta_i^2)/2R^2}, \end{aligned} \tag{10}$$

$$v_i = Y + \frac{(y_i - Y)\rho^2}{(x_i - X)^2 + (y_i - Y)^2}$$
$$= B + R\sin\theta + \frac{\rho^2}{2R}\frac{\sin\theta_i - \sin\theta + \delta_i/R}{1 - \cos(\theta_i - \theta) + \epsilon_i/R(\cos\theta_i - \cos\theta) + \delta_i/R(\sin\theta_i - \sin\theta) + (\epsilon_i^2 + \delta_i^2)/(2R^2)}. \quad (11)$$

When noise is absent ($\epsilon_i = \delta_i = 0$), we get

$$u_i = A + R\cos\theta + \frac{\rho^2}{2R}\frac{\cos\theta_i - \cos\theta}{1 - \cos(\theta_i - \theta)} \equiv u_{i0},$$

$$v_i = B + R\sin\theta + \frac{\rho^2}{2R}\frac{\sin\theta_i - \sin\theta}{1 - \cos(\theta_i - \theta)} \equiv v_{i0}.$$

In this situation, all the points (u_{i0}, v_{i0}) lie on the straight line Δ, the image of the inversion circle through the inversion transform, which passes through point P_*, orthogonal to PP_*.

Now we consider that noise is present in the data, but it is small in comparison with the radius of the circle: $|\epsilon_i| \ll R$, $|\delta_i| \ll R$. For the last terms of Eqs. (10) and (11) we can develop the linearized model given by first terms in the Taylor series and this suggests the following approximations:

$$u_i \approx A + R\cos\theta + \frac{\rho^2}{2R}\frac{\cos\theta_i - \cos\theta}{1 - \cos(\theta_i - \theta)}$$
$$+ \frac{\rho^2}{2R}\frac{\partial}{\partial x}\left[\frac{\cos\theta_i - \cos\theta + x}{1 - \cos(\theta_i - \theta) + x(\cos\theta_i - \cos\theta) + y(\sin\theta_i - \sin\theta) + (x^2 + y^2)/2}\right]\Bigg|_{x=0,y=0}\frac{\epsilon_i}{R}$$
$$+ \frac{\rho^2}{2R}\frac{\partial}{\partial y}\left[\frac{\cos\theta_i - \cos\theta + x}{1 - \cos(\theta_i - \theta) + x(\cos\theta_i - \cos\theta) + y(\sin\theta_i - \sin\theta) + (x^2 + y^2)/2}\right]\Bigg|_{x=0,y=0}\frac{\delta_i}{R},$$
$$v_i \approx B + R\sin\theta + \frac{\rho^2}{2R}\frac{\sin\theta_i - \sin\theta}{1 - \cos(\theta_i - \theta)} + \frac{\rho^2}{2R}\frac{\partial}{\partial x}\left[\frac{\sin\theta_i - \sin\theta + y}{1 - \cos(\theta_i - \theta) + x(\cos\theta_i - \cos\theta) + y(\sin\theta_i - \sin\theta) + (x^2 + y^2)/2}\right]\Bigg|_{x=0,y=0}\frac{\epsilon_i}{R}$$
$$+ \frac{\rho^2}{2R}\frac{\partial}{\partial y}\left[\frac{\sin\theta_i - \sin\theta + y}{1 - \cos(\theta_i - \theta) + x(\cos\theta_i - \cos\theta) + y(\sin\theta_i - \sin\theta) + (x^2 + y^2)/2}\right]\Bigg|_{x=0,y=0}\frac{\delta_i}{R}.$$

Thus we get

$$u_i \approx A + R\cos\theta + \frac{\rho^2}{2R}\frac{\cos\theta_i - \cos\theta}{1 - \cos(\theta_i - \theta)}$$
$$+ \frac{\rho^2}{2R}\left\{\frac{1}{1 - \cos(\theta_i - \theta)} - \frac{(\cos\theta_i - \cos\theta)^2}{[1 - \cos(\theta_i - \theta)]^2}\right\}\frac{\epsilon_i}{R}$$
$$- \frac{\rho^2}{2R}\left\{\frac{(\cos\theta_i - \cos\theta)(\sin\theta_i - \sin\theta)}{[1 - \cos(\theta_i - \theta)]^2}\right\}\frac{\delta_i}{R},$$

$$v_i \approx B + R\sin\theta + \frac{\rho^2}{2R}\frac{\sin\theta_i - \sin\theta}{1 - \cos(\theta_i - \theta)}$$
$$- \frac{\rho^2}{2R}\left\{\frac{(\sin\theta_i - \sin\theta)(\cos\theta_i - \cos\theta)}{[1 - \cos(\theta_i - \theta)]^2}\right\}\frac{\epsilon_i}{R}$$
$$+ \frac{\rho^2}{2R}\left\{\frac{1}{1 - \cos(\theta_i - \theta)} - \frac{(\sin\theta_i - \sin\theta)^2}{[1 - \cos(\theta_i - \theta)]^2}\right\}\frac{\delta_i}{R}.$$

We can now write:

$$u_i \approx u_{i0} + u_{i\epsilon}\frac{\epsilon_i}{R} + u_{i\delta}\frac{\delta_i}{R},$$

$$v_i \approx v_{i0} + v_{i\epsilon}\frac{\epsilon_i}{R} + u_{i\delta}\frac{\delta_i}{R},$$

where

$$u_{i\epsilon} = \frac{\rho^2}{2R}\left\{\frac{1}{1 - \cos(\theta_i - \theta)} - \frac{(\cos\theta_i - \cos\theta)^2}{[1 - \cos(\theta_i - \theta)]^2}\right\},$$

$$u_{i\delta} = -\frac{\rho}{2R}\left\{\frac{(\cos\theta_i - \cos\theta)(\sin\theta_i - \sin\theta)}{[1 - \cos(\theta_i - \theta)]^2}\right\},$$

$$v_{i\epsilon} = -\frac{\rho^2}{2R}\left\{\frac{(\sin\theta_i - \sin\theta)(\cos\theta_i - \cos\theta)}{[1 - \cos(\theta_i - \theta)]^2}\right\},$$

$$v_{i\delta} = \frac{\rho^2}{2R}\left\{\frac{1}{1 - \cos(\theta_i - \theta)} - \frac{(\sin\theta_i - \sin\theta)^2}{[1 - \cos(\theta_i - \theta)]^2}\right\}.$$

In the following, we shall compute the distance between the point (u_i,v_i) and straight line Δ. Because both points (X_*,Y_*) and (u_{i0},v_{i0}) lie on Δ, we have the following relationship for the distance between the point (u_i,v_i) and straight line Δ:

$$\frac{(u_{i0}-X_*)(v_i-v_{i0})-(v_{i0}-Y_*)(u_i-u_{i0})}{[(X_*-u_{i0})^2+(Y_*-v_{i0})^2]^{1/2}},$$

which gives us

$$\frac{\left[\frac{\cos\theta_i-\cos\theta}{1-\cos(\theta_i-\theta)}+\cos\theta\right]\left(v_{i\epsilon}\frac{\epsilon_i}{R}+v_{i\delta}\frac{\delta_i}{R}\right)-\left[\frac{\sin\theta_i-\sin\theta}{1-\cos(\theta_i-\theta)}+\sin\theta\right]\left(u_{i\epsilon}\frac{\epsilon_i}{R}+u_{i\delta}\frac{\delta_i}{R}\right)}{\left\{\left[\frac{\cos\theta_i-\cos\theta}{1-\cos(\theta_i-\theta)}+\cos\theta\right]^2+\left[\frac{\sin\theta_i-\sin\theta}{1-\cos(\theta_i-\theta)}+\sin\theta\right]^2\right\}^{1/2}},$$

and consequently

$$\frac{\left[\frac{\sin(\theta_i-\theta)\sin\theta}{1-\cos(\theta_i-\theta)}\right]\left(v_{i\epsilon}\frac{\epsilon_i}{R}+v_{i\delta}\frac{\delta_i}{R}\right)-\left[\frac{\sin(\theta_i-\theta)\cos\theta}{1-\cos(\theta_i-\theta)}\right]\left(u_{i\epsilon}\frac{\epsilon_i}{R}+u_{i\delta}\frac{\delta_i}{R}\right)}{\left\{\left[\frac{\sin(\theta_i-\theta)\sin\theta}{1-\cos(\theta_i-\theta)}\right]^2+\left[\frac{\sin(\theta_i-\theta)\cos\theta}{1-\cos(\theta_i-\theta)}\right]^2\right\}^{1/2}}=\sin\theta\left(v_{i\epsilon}\frac{\epsilon_i}{R}+v_{i\delta}\frac{\delta_i}{R}\right)-\cos\theta\left(u_{i\epsilon}\frac{\epsilon_i}{R}+u_{i\delta}\frac{\delta_i}{R}\right).$$

We introduce now the couples $(\hat{u}_i,\hat{v}_i)$, which are the closest points on the line Δ for a particular data point (u_i,v_i). This results that the sum of square distances of the data points to the straight line Δ is

$$\begin{aligned}
&\sum_{i=1}^{N}[(u_i-\hat{u}_i)^2+(v_i-\hat{v}_i)^2]\\
&\quad=\sum_{i=1}^{N}\left[\sin\theta\left(v_{i\epsilon}\frac{\epsilon_i}{R}+v_{i\delta}\frac{\delta_i}{R}\right)-\cos\theta\left(u_{i\epsilon}\frac{\epsilon_i}{R}+u_{i\delta}\frac{\delta_i}{R}\right)\right]^2\\
&\quad=\sin^2\theta\sum_{i=1}^{N}\left(v_{i\epsilon}\frac{\epsilon_i}{R}+v_{i\delta}\frac{\delta_i}{R}\right)^2\\
&\qquad+\cos\theta\sum_{i=1}^{N}\left(u_{i\epsilon}\frac{\epsilon_i}{R}+u_{i\delta}\frac{\delta_i}{R}\right)^2\\
&\qquad-2\sin\theta\cos\theta\sum_{i=1}^{N}\left(v_{i\epsilon}\frac{\epsilon_i}{R}+v_{i\delta}\frac{\delta_i}{R}\right)\left(u_{i\epsilon}\frac{\epsilon_i}{R}+u_{i\delta}\frac{\delta_i}{R}\right).
\end{aligned}$$

The weights $u_{i\epsilon}$, $u_{i\delta}$, $v_{i\epsilon}$, and $v_{i\delta}$ show how the noise contribute to the distances of the inversion points (u_i,v_i) to the straight line Δ. Ordinary plots of these weights with respect to angle θ_i for $\theta=0$ are shown in Fig. 5. We can conclude that when the scattered point is close to the pole of inversion, the influence of noise is destructive in both u and v coordinates, for any nonzero ϵ_i or δ_i. This can be easily justify if we take into consideration the fact that all the parameters $u_{i\epsilon}$, $u_{i\delta}$, $v_{i\epsilon}$, and $v_{i\delta}$ goes to infinity when $\theta_i\to\theta$ as $(\theta_i-\theta)^{-2}$.

4 Proposed Iterative Weighted Inversion Method

Based on previous observations it becomes clear that the points have to be treated differently and according with their distances to the pole. A possibility is to associate different weights w_i with given observation points M_i and after that to slightly modify the inversion method. But before we shall briefly follow[13] to recall the solution for weighted total least squares.

4.1 *Weighted Total Least Squares*

Now our aim is to minimize, over all a and b, the quantity

$$J(a,b)=\sum_{i=1}^{N}w_i[(u_i-\hat{u}_i)^2+(v_i-\hat{v}_i)^2],$$

where w_i are certain weights. As before the point $(\hat{u}_i,\hat{v}_i)$ is the closest point on a line $v=a+bu$ for a particular data point (u_i,v_i). Its coordinates are

$$\hat{u}_i=\frac{bv_i+u_i-ab}{1+b^2},\quad \hat{v}_i=a+b\,\frac{bv_i+u_i-ab}{1+b^2}.$$

We have

$$\begin{aligned}
J(a,b)&=\sum_{i=1}^{N}w_i[(u_i-\hat{u}_i)^2+(v_i-\hat{v}_i)^2]\\
&=\sum_{i=1}^{N}w_i\left\{\frac{b^2}{(1+b^2)^2}[v_i-(a+bu_i)]^2+\frac{1}{(1+b^2)^2}\right.\\
&\qquad\left.\times[v_i-(a+bu_i)]^2\right\}\\
&=\sum_{i=1}^{N}w_i\frac{1}{(1+b^2)^2}[v_i-(a+bu_i)]^2. \qquad (12)
\end{aligned}$$

For fixed b, the term in front of the sum is constant, thus the minimizing choice of a in the sum is

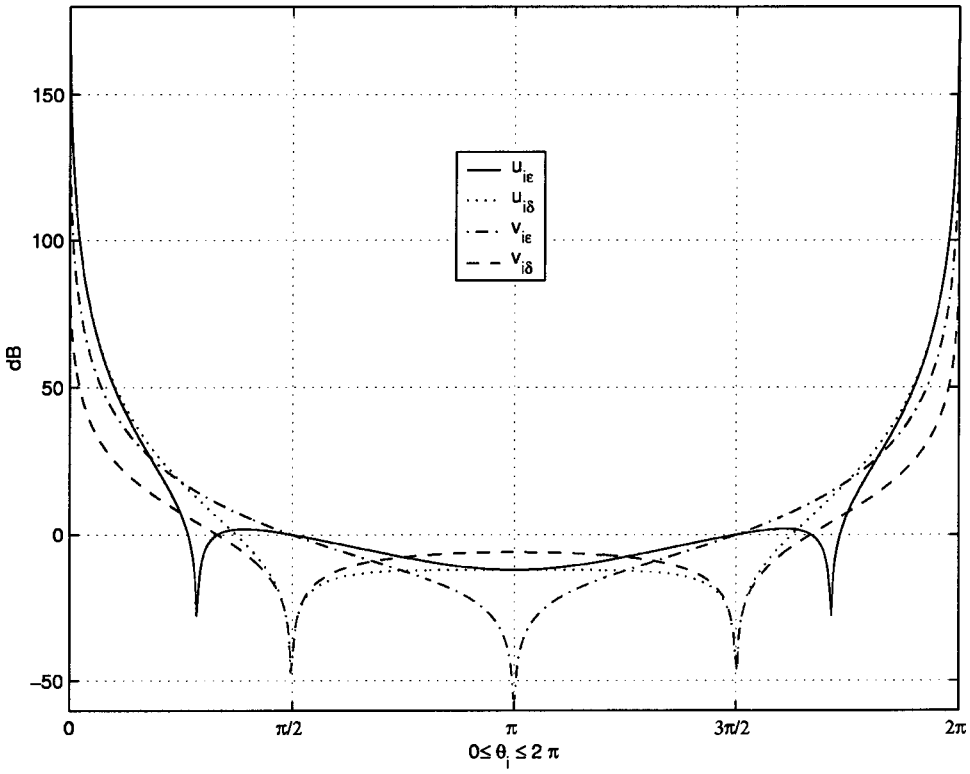

Fig. 5 Parameters $u_{i\epsilon}$, $u_{i\delta}$, $v_{i\epsilon}$, and $v_{i\delta}$ as functions of variable θ_i for $\theta=0$.

$$a=\frac{\Sigma_{i=1}^{N} w_i v_i}{\Sigma_{i=1}^{N} w_i}-b\frac{\Sigma_{i=1}^{N} w_i u_i}{\Sigma_{i=1}^{N} w_i},$$

or $a=\overline{v}^*-b\overline{u}^*$, where

$$\overline{u}^*=\frac{\Sigma_{i=1}^{N} w_i u_i}{\Sigma_{i=1}^{N} w_i}, \quad \overline{v}^*=\frac{\Sigma_{i=1}^{N} w_i v_i}{\Sigma_{i=1}^{N} w_i}. \tag{13}$$

Substituting back into the sum of Eq. (12), the weighted total least-squares solution is the one that minimizes, over all b:

$$\frac{1}{1+b^2}\sum_{i=1}^{N} w_i[(v_i-\overline{v}_i^*)-b(u_i-\overline{u}_i^*)]^2. \tag{14}$$

Now we define the following weighted sum of squares and cross-products by

$$S_{uu}=\sum_{i=1}^{N} w_i(u_i-\overline{u}^*)^2, \quad S_{uu}=\sum_{i=1}^{N} w_i(u_i-\overline{u}^*)(v_i-\overline{v}^*), \tag{15}$$

$$S_{vv}=\sum_{i=1}^{N} w_i(v_i-\overline{v}^*)^2.$$

Expanding the square and summing shows that Eq. (14) becomes

$$\frac{S_{vv}-2bS_{uv}+b^2S_{uu}}{1+b^2},$$

which will give the minimum[13] for

$$b=\frac{-(S_{uu}-S_{vv})+[(S_{uu}-S_{vv})^2+4S_{uv}^2]^{1/2}}{2S_{uv}}.$$

In this way, to find the estimated straight line we can use the same formula of Eq. (4), but where Eq. (5) is modified to Eqs. (13) and (15).

4.2 *Weighted Inversion Method*

Now we can present the algorithm which fits to a circle some scattered points using the weighted inversion (WI) transformation method:
(WI-1)≡(I-1),
(WI-2)≡(I-2),
(WI-3) Compute the parameters a and b of their fitted straight line using Eqs. (4), (13), and (15),
(WI-4)≡(I-4),
where (I-1), (I-2), and (I-4) are the corresponding steps from the inversion transformation method. The weight w_i has to be related to $\theta_i-\theta$ and should satisfy the following requirement: w_i goes to zero when $\theta_i\rightarrow\theta$ at least as $(\theta_i-\theta)^{\alpha}$, with $\alpha\geqslant 2$.

This condition tries to minimize the noise effect through the parameters $u_{i\epsilon}$, $u_{i\delta}$, $v_{i\epsilon}$, and $v_{i\delta}$. The distance between the data point and the inversion pole $[(x_i-X)^2+(y_i-Y)^2]$ is somehow related to the difference $\theta_i-\theta$, thus w_i might be selected one of the monotonic increasing functions of distance.

4.2.1 *Example 3: Example 2 revisited.*

We reconsider Example 2 with the same framework and simulation parameters. We only modify the step (I-3) to (WI-3) and we select

$$w_i=[(x_i-X)^2+(y_i-Y)^2]^r,$$

where the exponent r is changed during tests for different experiments from 0 (no weighting at all) to 0.5, 1, 1.5, 2, 2.5, 3, and 3.5 (weighting with the different first to seventh power of the distance). The outcomes are presented in Fig. 6 and Table 2. We can see that the best choice is to weight with the fourth power of the distance.

Remark 1. This result is consistent with the requirement on weight w_i and the fact that the square of distance is proportional with $(\theta_i-\theta)^2$.

Indeed we have the following expression for the weighted total least squares:

$$\begin{aligned}
&\sum_{i=1}^{N} w_i[(u_i-\hat{u}_i)^2+(v_i-\hat{v}_i)^2] \\
&\quad=\sum_{i=1}^{N} w_i\left[\sin\theta\left(v_{i\epsilon}\frac{\epsilon_i}{R}+v_{i\delta}\frac{\delta_i}{R}\right)\right. \\
&\quad\quad\left.-\cos\theta\left(u_{i\epsilon}\frac{\epsilon_i}{R}+u_{i\delta}\frac{\delta_i}{R}\right)\right]^2 \\
&\quad=\sin^2\theta\sum_{i=1}^{N} w_i\left(v_{i\epsilon}\frac{\epsilon_i}{R}+v_{i\delta}\frac{\delta_i}{R}\right)^2 \\
&\quad\quad+\cos^2\theta\sum_{i=1}^{N} w_i\left(u_{i\epsilon}\frac{\epsilon_i}{R}+u_{i\delta}\frac{\delta_i}{R}\right)^2 \\
&\quad\quad-2\sin\theta\cos\theta\sum_{i=1}^{N} w_i\left(v_{i\epsilon}\frac{\epsilon_i}{R}+v_{i\delta}\frac{\delta_i}{R}\right) \\
&\quad\quad\times\left(u_{i\epsilon}\frac{\epsilon_i}{R}+u_{i\delta}\frac{\delta_i}{R}\right). \qquad (16)
\end{aligned}$$

On the other hand, the distance between the data point and the inversion pole can be written as

$$\begin{aligned}
(x_i-X)^2+(y_i-Y)^2&=1-\cos(\theta_i-\theta)+\frac{\epsilon_i}{R}(\cos\theta_i-\cos\theta) \\
&\quad+\frac{\delta_i}{R}(\sin\theta_i-\sin\theta)+\frac{\epsilon_i^2+\delta_i^2}{2R^2},
\end{aligned}$$

and we have

$$\begin{aligned}
w_i&=[(x_i-X)^2+(y_i-Y)^2]^r \\
&=\left[1-\cos(\theta_i-\theta)+\frac{\epsilon_i}{R}(\cos\theta_i-\cos\theta)+\frac{\delta_i}{R}(\sin\theta_i-\sin\theta)+\frac{\epsilon_i^2+\delta_i^2}{2R^2}\right]^r \\
&\approx\begin{cases}2^r\sin^r\dfrac{\theta_i-\theta}{2}\left[\sin\dfrac{\theta_i-\theta}{2}-\dfrac{\epsilon_i}{R}\sin\dfrac{\theta_i+\theta}{2}+\dfrac{\delta_i}{R}\cos\dfrac{\theta_i+\theta}{2}\right]^r & \theta_i\approx\theta, \\ [1-\cos(\theta_i-\theta)]^r & \text{otherwise,}\end{cases}
\end{aligned}$$

which justifies the remark.

With respect to Fig. 7, let us consider the following points:

$M_i(x_i,y_i)=$ data points

$N_i(u_i,v_i)=$ image under inversion of M_i

$\hat{N}_i(\hat{u}_i,\hat{v}_i)=$ orthogonal projection of N_i on straight line Δ

$\hat{M}_i(\hat{x}_i,\hat{y}_i)=$ the point where the $P\hat{N}$ meets the circle with center $O(A,B)$ and radius R.

We designate also by $\hat{\Delta}$ the perpendicular to Δ on $\hat{N}_i$. According to Ref. 16, we have:

$$N_i\hat{N}_i=\frac{\rho^2 M_i\hat{M}_i}{PM_iP\hat{M}_i}.$$

Now let us consider the expression used in first sum from Eq. (16) with the fourth power of distance. We can conclude that actually $w_i[(u_i-\hat{u}_i)^2+(v_i-\hat{v}_i)^2]$ is

$$w_iN_i\hat{N}_i^2=PM_i^4N_i\hat{N}_i^2\approx\rho^4M_i\hat{M}_i^2,$$

if M_i is very close to the given circle $[O(A,B);R]$. Thus when we minimize the proposed weighted least-squares, in fact we minimized the sum of $M_i\hat{M}_i^2$.

It remains to justify the significance of the distance $M_i\hat{M}_i$. It is easy to see that both M_i and $\hat{M}_i$ will lie on the same circle which passes through P and is the image under inversion of $\hat{\Delta}$. But because Δ and $\hat{\Delta}$ are orthogonal, their corresponding circles will be also orthogonal.[17] This means that the distance $M_i\hat{M}_i$ is nothing else that the length of the arc $(M_i\approx\hat{M}_i)$ from the point M_i to the inversion circle measured along the orthogonal circle to the inversion circle that passes through M_i. It follows that the cost function that can be associated to the proposed weighted inversion method is different from both least squares and Kasa cost functions. However,[‡]

1. When the point M_i is opposed to the pole of inversion, the given distance approaches the geometric distance to the circle and we get ordinary least-squares cost function.
2. When the point M_i is close to the pole of inversion, the given distance is rather equal with the length of the tangent and we retrieve a new cost function similar with the Kasa cost function, the only difference consists in that the Kasa cost function uses the fourth power of the tangent, and here we have only the second power.

When the noise is absent {i.e., when the data points lie on the same circle $[O(A,B);R]$}, the new cost function will be zero, as any distance from the data points to the circle is zero. It follows that for such a configuration and when the inversion pole lie on the same circle, by applying the weighted inversion transformation method we recover the

[‡]Note that the new cost function is proportional to the square of the distance $M_i\hat{M}_i$ only when the data points are close to the given circle, otherwise the new cost function becomes more complicated.

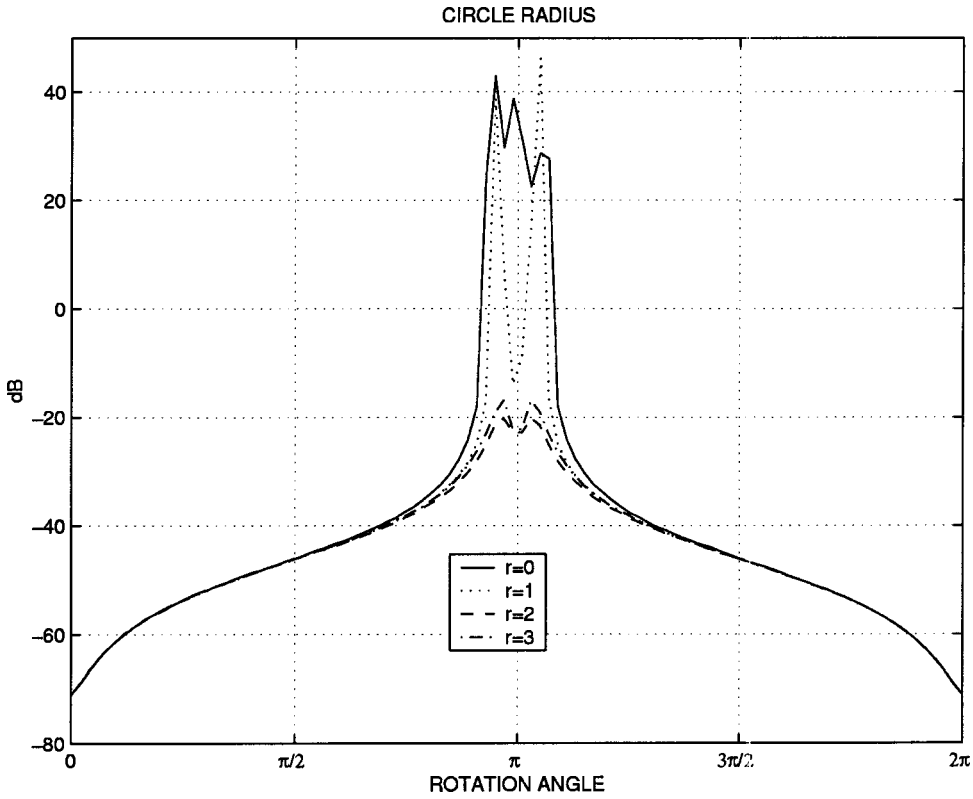

Fig. 6 MSE in decibels of the circle fitted radius for different rotation angles of scattered points and weight exponents.

initial circle. Thus the fitted procedure is exact. This fact we have verified also by simulations. However, when the inversion pole does not belong to the same circle as the data points, we have a different situation.

Let us consider now the pairs of points in Table 3. We can easily see that they are invariant to the inversion transformation with parameter ρ and pole of inversion (0,0). But when we want to compute the corresponding straight line for either least-squares or weighted least-squares methods we get a singularity issue. Such an inconvenient appears every time when the configuration is symmetric after inversion transformation and thus it provides us a straight line that passes through the pole of inversion. In this case, both inversion transformation and weighted transformation methods fail.

Another critical situation might appear when the parameter of inversion is very small. For that let us consider the expression used in last sum from Eq. (12) with the fourth power of distance. Using Eq. (3) we get

$$J(a,b) = \sum_{i=1}^{N} \frac{\{(Y-a-bX)[(x_i-X)^2+(y_i-Y)^2]+[(y_i-Y)-b(x_i-X)]\rho^2\}^2}{(1+b^2)^2},$$

and it can be approximated as follows:

$$J(a,b) \approx \frac{(Y-a-bX)^2}{(1+b^2)^2} \sum_{i=1}^{N} [(x_i-X)^2+(y_i-Y)^2]^2,$$

if $\rho \ll R$. The minimum of $J(a,b)$ is obtained for $Y-a-bX=0$, i.e., the pole of inversion will be on the fitted straight line. In this case, the weighted inversion method will also collapse.

4.3 *Iterative Weighted Inversion Method*

To reduce the influence given by the choice of inversion pole and to release the constrain that circle should pass through one given point, we propose an iterative algorithm by changing at every step the pole of inversion. However, this modification should not alter a ''good'' fitted circle if it has been already found. Thus our guess is to choose as the next pole of inversion the point that is diametrically opposite to the previous one.

Table 2 The maximum MSE in decibels of the circle fitted parameters (the radius and the center of the circles) for different error exponents.

r	MSE of Radius	MSE of Center
0	43.0491	43.0496
0.5	39.2911	39.2935
1	46.3189	46.3198
1.5	−18.0409	−17.9724
2	−20.1099	−20.0624
2.5	−18.9739	−18.9263
3	−16.7982	−16.7506
3.5	−13.9914	−13.9455

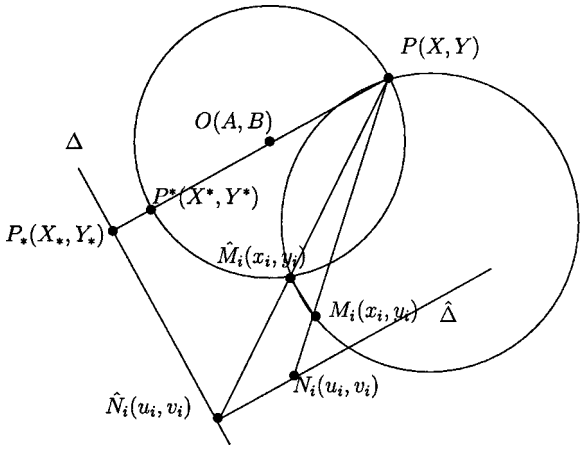

Fig. 7 Geometrical interpretation of the weighted inversion method.

The algorithm which estimates a circle using the iterative weighted inversion transformation method can be written as follows:

(IWI-O) Given

N = number of points

$M_i(x_i, y_i)$ = data to be fitted by circle

ρ = parameter of the inversion transformation

$k=1$

$P^{(1)}[X^{(1)}, Y^{(1)}]$ = first pole of inversion transformation

(IWI-k) while (stopping criterion $>\epsilon$) do:

(a) Compute the data $N_i^{(k)}[u_i^{(k)}, v_i^{(k)}]$ in the uv plane with:

$$u_i^{(k)} = X^{(k)} + \frac{[x_i - X^{(k)}]\rho^2}{[x_i - X^{(k)}]^2 + [y_i - Y^{(k)}]^2},$$

$$v_i^{(k)} = Y^{(k)} + \frac{[y_i - Y^{(k)}]\rho^2}{[x_i - X^{(k)}]^2 + [y_i - Y^{(k)}]^2}.$$

(b) Compute the weights w_i:

$$w_i = \{[x_i - X^{(k)}]^2 + [y_i - Y^{(k)}]^2\}^2.$$

(c) Compute the parameters a and b of their fitted straight line $v = a + bu$ using

$$a = \overline{v} - b\overline{u},$$

$$b = \frac{-(S_{uu} - S_{vv}) + [(S_{uu} - S_{vv})^2 + 4S_{uv}^2]^{1/2}}{2S_{uv}},$$

where

$$\overline{u} = \frac{\sum_{i=1}^N w_i u_i^{(k)}}{\sum_{i=1}^N w_i}, \quad \overline{v} = \frac{\sum_{i=1}^N w_i v_i^{(k)}}{\sum_{i=1}^N w_i},$$

$$S_{uu} = \sum_{i=1}^N w_i [u_i^{(k)} - \overline{u}]^2,$$

$$S_{uv} = \sum_{i=1}^N w_i [u_i^{(k)} - \overline{u}][v_i^{(k)} - \overline{v}],$$

$$S_{uv} = \sum_{i=1}^N w_i [v_i^{(k)} - \overline{v}]^2.$$

(d) Find the fitted circle $C(k)$ that corresponds to the fitted straight line. The steps are the following:

(i) For the given pole of inversion $P^{(k)}[X^{(k)}, Y^{(k)}]$ we have a certain point $P_{**}^{(k)}[X_{**}^{(k)}, Y_{**}^{(k)}]$ on a line $Y = a + bX$ that is closest when we measure distance orthogonally:

$$X_{**}^{(k)} = \frac{bY^{(k)} + X^{(k)} - ab}{1 + b^2},$$

$$Y_{**}^{(k)} = a + b\frac{bY^{(k)} + X^{(k)} - ab}{1 + b^2}.$$

(ii) The corresponding image point of $P_{**}^{(k)}[X_{**}^{(k)}, Y_{**}^{(k)}]$ by using I^{-1} is exactly $P_{(k)}^{**}[X_{(k)}^{**}, Y_{(k)}^{**}]$, the new diametrically opposite in the circle $C(k)$ to the $P^{(k)}[X^{(k)}, Y^{(k)}]$:

$$X_{(k)}^{**} = X^{(k)} + \frac{[X_{**}^{(k)} - X^{(k)}]\rho^2}{[X_{**}^{(k)} - X^{(k)}]^2 + [Y_{**}^{(k)} - Y^{(k)}]^2},$$

$$Y_{(k)}^{**} = Y^{(k)} + \frac{[Y_{**}^{(k)} - Y^{(k)}]\rho^2}{[X_{**}^{(k)} - X^{(k)}]^2 + [Y_{**}^{(k)} - Y^{(k)}]^2}.$$

(iii) The fitted circle is described by the coordinates of the center $[A^{(k+1)}, B^{(k+1)}]$ and the radius $R^{(k+1)}$:

$$A^{(k+1)} = \frac{X^{(k)} + X_{(k)}^{**}}{2}, \quad B^{(k+1)} = \frac{Y^{(k)} + Y_{(k)}^{**}}{2},$$

$$R^{(k+1)} = \{[X^{(k)} - A^{(k+1)}]^2 + [Y^{(k)} - B^{(k+1)}]^2\}^{1/2}.$$

(e) The new inversion pole is $P^{(k+1)}[X^{(k+1)}, Y^{(k+1)}]$, where $[X^{(k+1)}, Y^{(k+1)}] \equiv [X_{(k)}^{**}, Y_{(k)}^{**}]$.

(f) $k = k + 1$.

(g) Compute the stopping criterion: $\{[X^{(k+1)} - Y^{(k-1)}]^2 + [Y^{(k+1)} - Y^{(k-1)}]^2\}^{1/2}$.

In our experiments we used $\epsilon = 10^{-3}$.

Table 3 Pairs of points.

x	ρ	0	$-\rho$	0
y	0	ρ	0	$-\rho$

4.4 *Experimental Results*

The evaluation of the proposed approach of circle fitting has been performed on the artificial data sets shown in

Table 4 The coordinates of the points included into the experimental data sets.

	$\mathcal{A}$		$\mathcal{B}$		$\mathcal{C}$	
Point	x	y	x	y	x	y
1	−0.7783	21.4885	1.0000	7.0000	0.2655	0.7680
2	14.6672	6.7159	2.0000	6.0000	0.4002	0.9630
3	−8.3475	−13.7310	5.0000	8.0000	0.8819	0.6398
4	−6.8840	−14.5970	7.0000	7.0000	1.0567	0.1867
5	13.4167	−7.7091	9.0000	5.0000	0.1744	1.0433
6	−16.0429	9.2865	3.0000	7.0000	0.6058	0.8006
7	−24.1829	−0.8947	6.0000	2.0000	-	-
8	8.9161	−18.3074	8.0000	4.0000	-	-

Table 4. The data sets $\mathcal{A}$ and $\mathcal{B}$ have been adopted from the paper[18] by Gander *et al.* The points included in these two data sets are distributed over almost the entire circumference of certain generating circles. On the other hand, the six points in the set $\mathcal{C}$ have been randomly selected in the neighborhood of the unity circle ($A=B=0, R=1$) such that to cover only a quarter of the circumference.

The parameters of the circles determined for the three data sets using different circle fitting approaches are shown in Table 5. These results reveal that our method converges to a solution close to the solution offered by ODR algorithm. In addition, we may note that for the set $\mathcal{C}$, both algorithms found solutions that represent good approximations of the actual circle used to generate the observation points. Visual comparisons between the circles determined by different methods are shown in Figs. 8 and 9. From Fig. 9 we can note that both the algebraic method and Kasa method fail to determine a good approximation of the unity circle used to generate the points in set $\mathcal{C}$.

Another set of experiments was conducted to evaluate the efficiency of our algorithm in comparison with the ODR algorithm. The efficiency was expressed by the number of iterations as well as by the number of floating point operations (flops) performed by both algorithms to estimate the circles that fit each one of the three experimental data sets. The algebraic circle has been used in our experiments to provide the initial parameters of ODR algorithm, and the initial inversion pole required by our algorithm was chosen as one of the observed points. The results obtained are shown in Table 6. From these results, we can note that for all three data sets our method overcomes in efficiency the ODR algorithm regardless of the point selected as the initial inversion pole.

The selection of the initial inversion pole is not restricted to the points in the given set. We determined the number of iterations required for different positions of the initial inversion pole in a restricted domain around the observed points. The results are shown in Fig. 10 for the data sets $\mathcal{A}$ and $\mathcal{B}$. We can note that the number of iterations for the data sets $\mathcal{A}$ and $\mathcal{B}$ does not exceed 10 and 21, respectively, if the initial pole is selected in the neighborhood of the given points. As expected an ideal position for the initial pole would be onto the circle that follows to be estimated. On the other hand, note that an unfavorable region for the initial pole occurs close to the centroid of the given set of points.

Note that the proposed algorithm does not converge for any position of the initial inversion pole. This is reflected by the plots shown in Fig. 11, where the initial pole was chosen at relative large distances from the given set of points.

We now try to explain this behavior. After a certain number of iterations the pole of inversion can be in the middle of the cloud generated by the scattered points. In this case, we can retrieve a situation similar to that mentioned at the end of Sec. 4.1, i.e., by applying the inversion transform we get a configuration where the fitted straight line passes through the pole of inversion or in its very close neighborhood. The weighted inversion method can reduce the effect using different weights for different points, but when all the points are very close to the pole of inversion or identically, it fails. However, when the starting pole of inversion is one of the scattered points, usually there is enough place for other further points to trace a good starting circle, and in this case, the procedure converges to the fitted circle. Unfortunately this is not always possible, at least when the pole of inversion is far away from the scattered points, which returns on the next iteration a new pole of inversion quite in the middle of the data points. We performed simulations for different initialization data and

Table 5 The parameters of the circles determined with different approaches given the observed points in the three data sets.

	Data set $\mathcal{A}$			Data set $\mathcal{B}$			Data set $\mathcal{C}$		
Method	A	B	R	A	B	R	A	B	R
Our method	−2.19	1.32	19.17	4.77	4.77	3.54	0.09	−0.03	1.00
ODR	−1.93	1.53	18.73	4.84	4.80	3.39	0.10	−0.05	1.00
Kasa method	−2.21	1.19	18.82	4.82	4.90	3.41	0.41	0.36	0.59
Algebraic circle	−2.01	1.38	19.52	5.12	5.43	3.24	0.78	0.79	0.48

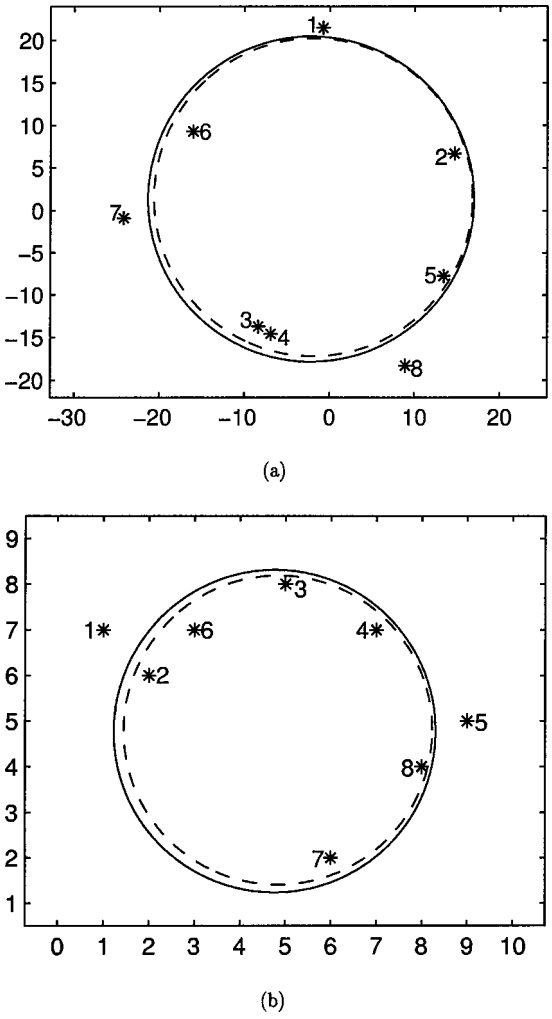

Fig. 8 Circles determined using our method (continuous line) and the ODR algorithm (dashed line) for the observation points (⋆) included in the data set $\mathcal{A}$ (a), and in the data set $\mathcal{B}$ (b).

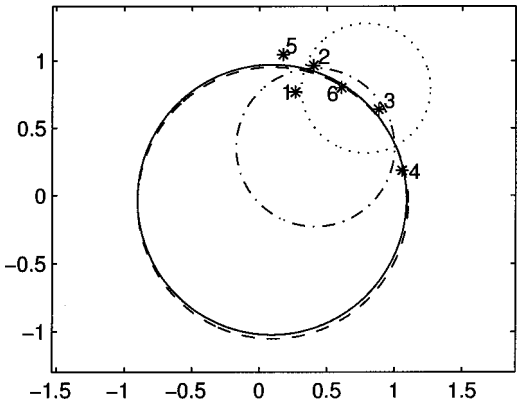

Fig. 9 Circles determined using our method (continuous line), the ODR algorithm (dashed line), the Kasa method (dash-dotted line), and the algebraic circle (dotted line) for the observation points (⋆) in the data set $\mathcal{C}$.

the results suggest that the region that is not convenient to start the iterative weighted inversion procedure is beside the centroid rather than its symmetric to the center of the generating circle, when they are different each other. If the scattered points are not symmetrically distributed, then the curvature of the generating circle and of the inversion circle should not be opposed.

Finally, we conducted a set of experiments to evaluate the behavior of the proposed approach in the presence of outliers. The experimental data sets used in these fitting experiments were created as follows. First 100 points were generated on a circle of radius 1 centered at the origin. Next the points were deviated from the circle by means ofGaussian noise with zero mean and standard deviation 0.1. Then a number of K outliers were randomly selected in the square $[-S,S]\times[-S,S]$. For each value of K and S we applied the proposed circle fitting algorithm on 1000 different experimental data sets generated in accordance to the

Table 6 The number of iterations and the number of floating point operations (flops) performed by both our method and ODR algorithm.

	Data Set $\mathcal{A}$		Data Set $\mathcal{B}$		Data Set $\mathcal{C}$	
Initial Pole	Iterations	flops/1000	Iterations	flops/1000	Iterations	flops/1000
Our Method (the initial inversion pole is one of the points in the given set)						
First point	5	6	4	5	4	3
Second point	6	7	3	3	7	6
Third point	6	7	9	11	12	10
Fourth point	6	7	9	11	5	4
Fifth point	5	6	5	6	3	2
Sixth point	5	6	4	5	13	11
Seventh point	6	7	6	7	—	—
Eighth point	6	7	3	3	—	—
ODR algorithm (the initial parameters are provided by the algebraic circle)						
—	41	83	27	53	178	313

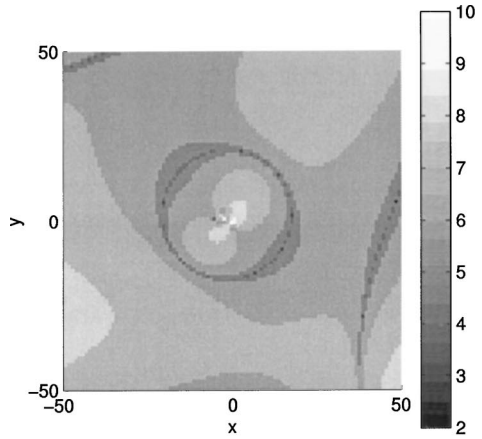

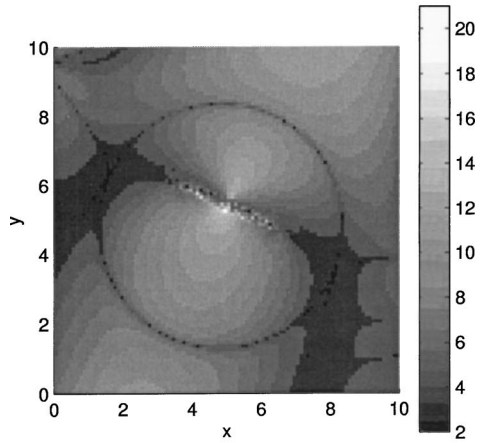

Fig. 10 Number of iterations as a function of the location selected for the initial inversion pole.

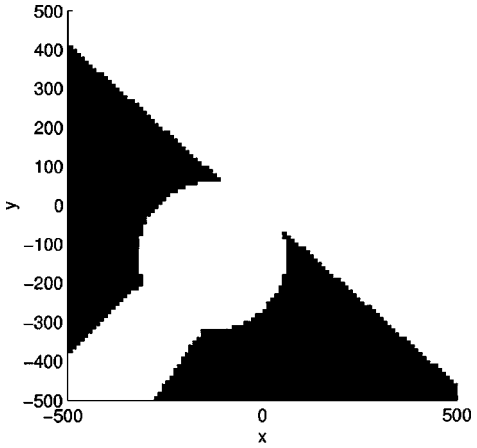

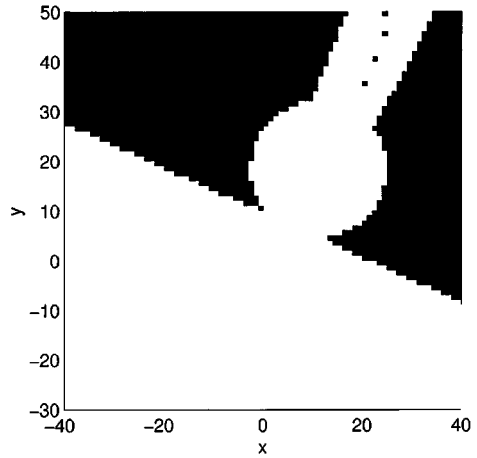

Fig. 11 Positions (black) of the initial inversion pole for which the algorithm does not converge.

procedure already described. The average distance between the estimated center position and the origin, as well as the average displacement between the estimated radius and the true radius (i.e., $R=1$) for different K and S are shown in Table 7. We conclude that the proposed method might be improved with approaches characteristic to robust statistics to achieve better results in the presence of outlier points.

5 Conclusions

We have proposed a new circle-fitting procedure based on a classical geometric result. First, we recalled the main approaches to circle fitting by emphasizing the inversion transformation method as it was first proposed by Brandon and Cowley. The weaknesses of this method was shown by examples and they have been proved by mathematical justifications. Then we have derived the weighted inversion transformation method that overcomes the inconvenience of inversion method being able to find a fitted circle when one point of the circle is given. To release the last constrain, an iterative procedure is finally proposed by changing the pole of inversion at every step. Our guess was to choose as the next pole of inversion the point that is diametrically opposite to the previous one. The experimental results showed that the proposed technique can be applied to both symmetrically and asymmetrically distributed data around the circumference of the circle. Thus the iterative weighted inversion method can be successfully applied when the Kasa method fails. In addition, the experimental results show that our method overcomes in efficiency the ODR algorithm.

Acknowledgments

The first author thanks Prof. Visa Koivunen and his group from Helsinki University of Technology for providing relevant references.

Table 7 The average displacements of the estimated center position (a) and the estimated radius (b), from the true circle, in the presents of outliers, where the parameters of the true circle are $A=B=0$ and $R=1$.

(a) and (b)	$K=0$	$K=5$	$K=10$	$K=15$
$S=1.5$	(0.09, 0.01)	(0.03, 0.03)	(0.04, 0.05)	(0.05, 0.07)
$S=2.0$	(0.09, 0.01)	(0.09, 0.10)	(0.12, 0.16)	(0.13, 0.21)
$S=2.5$	(0.09, 0.01)	(0.20, 0.20)	(0.23, 0.34)	(0.31, 0.42)

References

1. V. Pratt, ''Direct least-squares fitting of algebraic surfaces,'' *Comput. Graph.* **21**(4), 145–152 (1987).
2. J. Pegna and C. Guo, ''Computational metrology of the circle,'' in *IEEE Proc. Computer Graphics International*, pp. 350–363 (1998).
3. G. Vosselman and R. M. Haralick, ''Performance analysis of line and circle fitting in digital images,'' in *Proc. Workshop on Performance Characteristics of Vision Algorithms*, Cambridge (Apr. 1996).
4. M. Berman and P. I. Somlo, ''Efficient procedures for fitting circles and ellipses with application to sliding termination measurements,'' *IEEE Trans. Instrum. Meas.* **IM-35**(1), 31–35 (1986).
5. Z. Zhang, ''Parameter estimation techniques: a tutorial with applications to conic fitting,'' *Int. J. Image Vis. Comput.* **15**(1), 59–76 (1997).
6. G. N. Newsam and N. J. Redding, ''Fitting the most probable curve to noisy observations,'' in *IEEE Proc. ICIP'97*, pp. 752–755 (1997).
7. W. Gander, G. H. Golub, and R. Strebel, ''Least-squares fitting of circles and ellipses,'' *BIT* **34**, 558–578 (1994).
8. P. S. Modenov and A. S. Parkhomenko, *Geometric Transformations*, Academic Press, New York (1965).
9. J. A. Brandon and A. Cowley, ''A weighted least squares method for circle fitting to frequency response data,'' *J. Sound Vib.* **83**(3), 419–424 (1983).
10. I. Kasa, ''A circle fitting procedure and its error analysis,'' *IEEE Trans. Instrum. Meas.* , 8–14 (Mar. 1976).
11. N. I. Chernov and G. A. Ososkov, ''Effective algorithms for circle fitting,'' *Comput. Phys. Commun.* **33**, 329–333 (1984).
12. C. A. Corral and C. S. Lindquist, ''On implementing Kasa's circle fit procedure,'' *IEEE Trans. Instrum. Meas.* **47**(3), 789–795 (1998).
13. G. Casella and R. L. Berger, *Statistical Inference*, Duxburry Press, Belmont, CA (1990).
14. M. Berman and D. Culpin, ''The statistical behaviour of some least squares estimators of the centre and radius of a circle,'' *J. R. Stat. Soc. Ser. B. Methodol.* **48**, 183–196 (1986).
15. M. Berman, ''Large sample bias in least squares estimators of a circular arc center and its radius,'' *Comput. Vis. Graph. Image Process.* **45**, 126–128 (1989).
16. Th. Caronnet, *Exercise de geometrie—complements*, Librarie Vuibert, Paris (1946).
17. H. S. M. Coxeter and S. L. Greitzer, *Geometry Revisited*, The Mathematical Association of America, Yale University, (1967).
18. W. Gander, G. H. Golub, and R. Strebel, ''Fitting of circles and ellipses—least-squares solution,'' Technical Report 217, Institut fur Wisenschaftliches ETH Zurich, (June 1994).

Corneliu Rusu graduated in electronics and telecommunications in 1985 from Technical University of Cluj-Napoca (TUCN) and in mathematics in 1990 from Babes-Bolyai University of Cluj-Napoca. He received his PhD degree in electronics in 1996 from TUCN and his DrTech degree in signal and image processing from Tampere University of Technology in 2000. After graduation he was an engineer with IIRUC, Computer Systems Division, Cluj-Napoca. In 1991 he joined the Department of Electronics and Telecommunications, TUCN, where he is now a professor. From 1997 to 2000 he was with the Signal Processing Laboratory, Tampere University of Technology, Finland, and during the summer of 2001 he visited the Tampere International Center for Signal Processing. His research interests include adaptive filters, computer-aided analysis and synthesis of circuits, and image and optical information processing.

Marius Tico received his MSc degree in computer science and his PhD degree in electronics and telecommunications, both from Technical University of Cluj-Napoca, Romania, in 1993 and 1999, respectively, and his DrTech degree in signal and image processing from Tampere University of Technology, Finland, in 2001. From 1994 to 1997 he was a teaching assistant with the Department of Electronics and Telecommunications, the Technical University of Cluj-Napoca, Romania. From 1997 to 2001, he was a research engineer with the Institute of Signal Processing, Tampere University of Technology, Finland. Since December 2001, he has been a research engineer with Nokia Research Center, Tampere, Finland. His research interests include signal and image processing, pattern recognition, and biometrics.

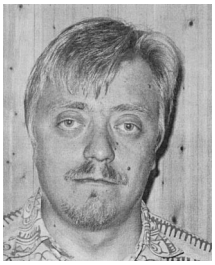

Pauli Kuosmanen received his BSc, MSc, and Licentiate degrees in mathematics from the University of Tampere, Finland, in 1989, 1991, and 1993, respectively, and his DrTech degree in signal processing from the Tampere University of Technology in 1994. Since 1990 he has held various research and teaching positions with the University of Tampere and the Tampere University of Technology. He is currently a part-time professor of signal processing. Since August 2001 he has directed New Technologies at the Research Center of the Elisa Communications Corp. Prof. Kuosmanen has authored over 90 international journal and conference papers, two international book chapters, and is a coauthor of the book *Fundamentals of Nonlinear Digital Filtering*. He has supervised several MSc and DrTech studends and led tens of research projects related to signal and image processing and digital media technology.

Edward J. Delp received his BSEE (cum laude) and MS degrees from the University of Cincinnati, his PhD degree from Purdue University, and an honorary DrTech degree from the Tampere University of Technology, Finland, in 2002. From 1980 to 1984 he was with the Department of Electrical and Computer Engineering, the University of Michigan, Ann Arbor, and since August 1984, he has been with the School of Electrical and Computer Engineering and the Department of Biomedical Engineering, at Purdue University, West Lafayette, Indiana. In 2002 he received a chaired professorship and currently is the Silicon Valley Professor of Electrical and Computer Engineering and Professor of Biomedical Engineering. During the summers of 1998, 1999, 2001, and 2002 he was a visiting professor with the Tampere International Center for Signal Processing, Tampere University of Technology, Finland. His research interests include image and video compression, multimedia security, medical imaging, multimedia systems, communication, and information theory. From 1997 to 1999 he chaired the Image and Multidimensional Signal Processing (IMDSP) Technical Committee of the IEEE Signal Processing Society and from 1994 to 1998 he was vice-president for publications of the Society of Imaging Science and Technology (IS&T). He cochaired SPIE/IS&T conferences on Security and Watermarking of Multimedia Contents in 1999, 2000, 2001, and 2002, was the general cochair of the 1997 Visual Communications and Image Processing Conference (VCIP) and the 1993 SPIE/IS&T Symposium on Electronic Imaging, program chair of the 1996 IEEE Signal Processing Society's Ninth IMDSP Workshop and is the program cochair of the 2003 IEEE International Conference on Image Processing. From 1984 to 1991 he was a member of the editorial board of the *International Journal of Cardiac Imaging*, from 1991 to 1993 an associate editor of the *IEEE Transactions on Pattern Analysis and Machine Intelligence*, from 1992 to 1999 a member of the editorial board of *Pattern Recognition*, from 1994 to 2000 an associate editor of the *Journal of Electronic Imaging*, and from 1996 to 1998 an associate editor of the *IEEE Transactions on Image Processing*. He received the Honeywell Award in 1990, D. D. Ewing Award in 1992, the Raymond C. Bowman in 2001, Award from IS&T in 2001, and a Nokia Fellowship in 2002. Dr. Delp is a fellow of the IEEE, SPIE, and IS&T and a member of Tau Beta Pi, Eta Kappa Nu, Phi Kappa Phi, Sigma Xi, ACM, and the Pattern Recognition Society. In 2000 he was selected a Distinguished Lecturer of the IEEE Signal Processing Society.